Biochimica et Biophysica Acta 1844 (2014) 1741–1748

Contents lists available at ScienceDirect

Biochimica et Biophysica Acta

journal homepage: www.elsevier.com/locate/bbapap

Crystal structure of serine acetyl transferase from *Brucella abortus* and its complex with coenzyme A

Sudhir Kumar [a,1], Nitesh Kumar [a], Neelima Alam [b], Samudrala Gourinath [a,*]

[a] School of Life Sciences, Jawaharlal Nehru University, New Delhi, Delhi 110067, India
[b] Technology Bhavan, Ministry of Science and Technology, New Mehrauli Road, New Delhi 110016, India

ARTICLE INFO

Article history:
Received 2 April 2014
Received in revised form 9 July 2014
Accepted 12 July 2014
Available online 22 July 2014

Keywords:
Brucella abortus
Serine acetyltransferase
Cysteine biosynthesis
Cysteine synthase complex

ABSTRACT

Brucella abortus is the major cause of premature foetal abortion in cattle, can be transmitted from cattle to humans, and is considered a powerful biological weapon. *De novo* cysteine biosynthesis is one of the essential pathways reported in bacteria, protozoa, and plants. Serine acetyltransferase (SAT) initiates this reaction by catalyzing the formation of *O*-acetylserine (OAS) using L-serine and acetyl coenzyme A as substrates. Here we report kinetic and crystallographic studies of this enzyme from *B. abortus*. The kinetic studies indicate that cysteine competitively inhibits the binding of serine to *B. abortus* SAT (BaSAT) and noncompetitively inhibits the binding of acetyl coenzyme A. The crystal structures of BaSAT in its apo state and in complex with coenzyme A (CoA) were determined to 1.96 Å and 1.87 Å resolution, respectively. BaSAT was observed as a trimer in a size exclusion column; however, it was seen as a hexamer in dynamic light scattering (DLS) studies and in the crystal structure, indicating it may exist in both states. The complex structure shows coenzyme A bound to the C-terminal region, making mostly hydrophobic contacts from the center of the active site extending up to the surface of the protein. There is no conformational difference in the enzyme between the apo and the complexed states, indicating lock and key binding and the absence of an induced fit mechanism.

1. Introduction

Sulfur assimilation in living systems is essential and is utilized in a number of downstream processes such as amino acid synthesis and various other metabolic pathways [1,2]. The cysteine biosynthetic pathway, found in bacteria, plants, and protist pathogens, is the first step of fixing inorganic sulfur into usable organic derivatives [3,4]. Serine is converted to *O*-acetylserine (OAS) by serine acetyltransferase (SAT, EC 2.3.1.30), which catalyzes the transfer of an acetyl group from acetyl coenzyme A to serine. This step is followed by the condensation of OAS with sulfide to form cysteine by *O*-acetylserine sulfhydrylase (OASS, EC 2.5.1.47). An alternate pathway also exists in some of the micro-organisms, e.g., *Mycobacterium tuberculosis*, where OASS uses O-phosphoserine as the substrate rather than *O*-acetylserine [5]. The first step is both rate limiting and subject to regulation as the end product cysteine feedback inhibits the SAT enzyme. A second mode of regulation is due to the association and dissociation of SAT and OASS, which form a cysteine synthase (CS) complex [6].

The crystal structures of *Escherichia coli* SAT (EcSAT) [7], *Haemophilus influenzae* SAT (HiSAT) [8], *Entamoeba histolytica* SAT (EhSAT) [9], and *Glycine max* SAT [10] have been previously published. The coordinates of a crystal structure of SAT from *Brucella melitensis* has also been deposited at the Protein Data Bank (PDB code: 3MC4). SATs from *E. coli, B. melitensis*, *H. influenzae, and G. max* were reported to form hexamers, while this enzyme from *E. histolytica* was reported as a trimer. SAT belongs to the *O*-acetyltransferase subfamily of acetyltransferases characterized by the presence of a unique hexapeptide repeat sequence [LIV]-[GAED]-X_2-[STAV]-X that results in the formation of a left-handed parallel β-helix (LβH) [7,11].

Brucella abortus, a Gram-negative intracellular blood-borne bacterium, is the major cause of brucellosis, which often results in premature abortion of the foetus in cattle [12]. It is primarily a zoonotic organism that can be transmitted from cattle to humans and is considered a powerful biological weapon [13]. In humans, when infected, *Brucella* resides and grows in side macrophages, thereby impairing the host immune system [14–16]. Currently available commercial vaccines are live and attenuated *Brucella* strains. Therefore, there is a need to identify new targets for development of single molecule or subunit vaccines [17] or lead molecules against probable targets.

There is relatively high similarity (47% to 99%) between the sequence of *B. abortus* SAT, and the sequences of other SATs for which crystal structures have been reported. Some of this similarity resides

* Corresponding author.
E-mail addresses: samudralag@yahoo.com, sgourinath@mail.jnu.ac.in (S. Gourinath).
[1] Present Address: Department of Zoology and Biotechnology, Hemwati Nandan Bahuguna Garhwal University, Srinagar, Uttarakhand 246174, India.

http://dx.doi.org/10.1016/j.bbapap.2014.07.009
1570-9639/

at the C-terminus, and the C-terminal residues of SAT bind to the active site of OASS, forming a cysteine synthase complex, which in turn reduces the activity of OASS [18]. Previous structural and biochemical studies have revealed that formation of cysteine synthase complexes requires SAT to have an isoleucine residue, at its C-terminal end [9]. The BaSAT C-terminal end sequence is Gly, Asp, Gly, and Ile, which should thus favor formation of the complex. BaSAT has been shown to completely inhibit *Leishmania donovanii* OASS [19], indicating that this SAT can form a cysteine synthase complex. OASS, as described above, is the second enzyme of pathway, and is structurally and biochemically well characterized in many organisms such as *E. coli* (PDB id 2BHT) [20], *M. tuberculosis* (PDB id 2Q3D) [21], *Arabidopsis thaliana* (PDB id 1Z7W) [22], and *E. histolytica* (PDB id 2PQM) [23].

Here we report the crystal structure of SAT from *B. abortus* strain S19, both in its apo (uncomplexed) state at a 1.97-Å resolution and in complex with CoA at a 1.87-Å resolution. Kinetic studies of BaSAT with serine as well as with acetyl CoA are also reported. The inhibition kinetics with final product cysteine shows competitive inhibition with substrate serine and mixed inhibition with acetyl coenzyme A. The structural, biophysical, and biochemical experiments indicate that BaSAT exists as a hexamer while gel filtration indicates a trimeric state. Comparison of apo and CoA complex crystal structures show there is no structural difference between them, indicating lock and key binding.

2. Materials and methods

2.1. Cloning, over-expression, and purification of B. abortus SAT

The cloning and over-expression of *B. abortus* SAT (BaSAT) is explained in detail in supplementary data. The over-expressed protein was purified using Ni-NTA column and gel filtration chromatography (Supplementary Fig. 1). The pure protein fractions were pooled and concentrated using Centricon concentrators (Amicon, Millipore) and taken for crystallization trials. The proteins were concentrated to 14 mg/ml in gel filtration elution buffer containing 50 mM Tris–HCl (pH 8.0), 150 mM NaCl, 5% glycerol, and 5 mM β-mercaptoethanol.

2.2. Crystallization of BaSAT

Crystallization trials of the purified BaSAT were carried out using various pre-formulated screens in 96-well plates (Molecular Dimensions, UK), with 100 μl of reservoir solution in each well. Hanging drops of 200 nl each of protein and precipitant were dispensed using the Mosquito™ (Molecular Dimensions, UK) crystallization robot (at Advanced Instrumentation Research Facility (AIRF), JNU, New Delhi) for vapor diffusion, and plates were incubated at 289 K or 277 K. The initial crystals were obtained using the Morpheus™ screen (Molecular Dimensions, UK). After replicating the conditions in 24-well plates (Hampton Research, USA) and optimizing various physicochemical parameters, the best crystals of BaSAT were obtained using 7% (w/v) PEG 1000, 7% (w/v) PEG 3350, 5% (v/v) MPD, 0.12 M ethylene glycol, 0.1 M Tris–HCl (pH 7.4), and 50 mM $MgCl_2$ at 289 K.

2.3. Crystallization of BaSAT in complex with CoA

BaSAT protein (14 mg/ml) was mixed with 0.1 mM coenzyme A (Sigma Aldrich, USA) and 2 mM L-serine prior to crystallization trials. Three microliters of protein and 3 μl of reservoir solution were mixed and allowed to equilibrate against the reservoir of 500 μl in 24-well plates. The best crystals appeared in the condition containing 5% PEG 1000, 5% PEG 1500, 5% MPD, 0.1 M ethylene glycol, 0.1 M Tris–HCl (pH 7.4), and 20–50 mM $MgCl_2$ at 289 K.

2.4. Data collection and processing

Crystals of BaSAT were equilibrated in cryo-solutions containing the crystallization condition but with concentrations of PEG 3350 increasing from 15% to 30%. These cryo-protected crystals were mounted in cryoloops, and initial data were collected at the AIRF, JNU, New Delhi, using a Bruker Microstar generator and MAR 345 imaging plate detector. High-resolution (up to 2 Å) diffraction data were collected at the DBT-European Synchrotron Radiation Facility beamline BM14. The data set was indexed, integrated, and scaled using the HKL-2000 data processing software [24]. BaSAT-coenzyme A complex crystal diffraction data were collected at the home source (AIRF, JNU). Data were indexed, integrated, and scaled using Automar (Mar-research, Germany) (Table 1).

2.5. Structure determination and refinement

The BaSAT structure was determined by the molecular replacement method using *B. melitensis* SAT as a search model (PDB id 3MC4, Abendroth et al., unpublished, Seattle Structural Genomics Center for Infectious Disease). This structure shares very high sequence similarity (~99%) with BaSAT. Crystals belonged to the $P2_1$ space group, and Matthews coefficient [25] calculations suggested that there could be twelve protomers in an asymmetric unit. Aligned sequences of *B. abortus* SAT and *Brucella melintensis* SAT were input into Chainsaw [26], and its output was used in the Molrep [27] module of CCP4 [28] for molecular replacement. A single protomer, trimer, and hexamer were used for molecular replacement. The latter yielded the best solution with lowest initial *R* value of 46.3% where two hexamers (a total of 12 protomers) were present in an asymmetric unit. A single step of 10 cycles of refinement in REFMAC5 [29] resulted in a decrease of the R_{work} to 21.9%. This model was further refined by rounds of iterative model building using the COOT graphics package [30] in combination with REFMAC5 and phenix.refine [31]. The remaining residues were built manually with COOT guided by the σ-weighted 2F*o*-F*c* and F*o*-F*c*

Table 1
Data collection and refinement statistics.

Data set	BaSAT-native	BaSAT-CoA
X-ray source	DBT-BM14, ESRF, France	Bruker Microstar
Wavelength (Å)	0.9787	1.54179
Space group	$P2_1$	R3
Unit cell parameters a, b, c (Å)	73.7, 256.8, 82.3	104.3, 104.3, 105.7
α, β, γ (°)	90.00, 91.20, 90.00	90.00, 90.00, 120.00
Resolution range (Å)	50–1.96 (1.99–1.96)	68.68–1.87 (1.92–1.87)
Completeness (%)	86.0 (83.0)	99.2 (92.3)
Unique HKLs	183943 (76642)	331387 (35422)
Multiplicity	2.4 (2.2)	9.18 (8.1)
Average <I/σI>	30.4 (2.9)	13.6 (1.8)
Crystal mosaicity (°)	0.6	0.45
R_{merge} (%)	3.8 (32.8)	6.8 (56.9)
Refinement		
R_{work} (%)	18.7	18.3
R_{free} (%)	24.3	23.4
Mean B factor (Å^2)		
Protein	36.5 (31.4 from Wilson plot)	29.4 (27.8 from Wilson plot)
CoA	–	67.2
Number of atoms		
Protein	22448	3788
Water	1158	149
CoA	–	48
Other	16	9
RMS deviations		
Bond length (Å)	0.013	0.013
Bond angles (°)	1.7	1.6
Ramachandran Plot Statistics		
Favored/allowed/disallowed (%)	96.4/3.4/0.2	97.8/2.2/0

The values in the parenthesis are for highest resolution shell. R_{free} was calculated using a randomly selected subset of 5% of the reflections.

electron density maps. Water molecules were initially identified using the ARP/wARP solvent program [32] and were subsequently checked manually by considering electron density and hydrogen bonding interactions with the protein. The final model is well refined, having R_{work} and R_{free} of 18.7% and 24.3%, respectively, and the phases from this model yield high-quality electron density (Supplementary Fig. 1d).

2.6. BaSAT-CoA complex structure

The protein–coenzyme A complex crystallized in the space group R3 with two protomers in an asymmetric unit. The (uncomplexed) BaSAT protomer structure was used as a search model for solving the BaSAT-CoA structure by molecular replacement. The initial model obtained from molecular replacement solution yielded a very good *R* value of 21.9%. The model was refined with Refmac5 and further improved by iterative model building using COOT. CoA was added from the COOT library guided by electron density in one of the monomers. The density for CoA in the other protomer was not good and didn't improve upon refinement. CoA was therefore only built in one protomer where electron density for the ligand improved with subsequent cycles of refinement. Although we added serine in the crystallization condition, we could not find any density corresponding to this amino acid.

2.7. Enzyme activity

BaSAT activity was calculated by monitoring the decrease in absorbance at 232 nm (A_{232}) due to the breakage of the thioester bond of acetyl coenzyme A using an Ultrospec 2100pro spectrophotometer (GE Healthcare). For this assay, the reaction mixture contained 50 mM Tris–HCl (pH 8.0), 0.1 mM acetyl-CoA, and 2.5 μg of BaSAT. The reaction was started by adding serine, and the absorbance was monitored every 2 s starting from zero. To calculate K_m for the binding of serine, the amino acid was added in varying concentrations from 10 to 500 μM, keeping the concentration of acetyl CoA constant at 0.1 mM, and the reaction was carried out at room temperature for 2 min. The K_m and the V_{max} values were calculated using the Michaelis–Menten curve. K_m was similarly calculated for acetyl Co-A, by varying acetyl Co-A from 10 to 400 μM and keeping the concentration of serine constant at 120 μM. Kinetic studies were performed in triplicate using 7–8 different concentrations of both serine and acetyl CoA. To measure the inhibition by L-cysteine, similar reactions were repeated using two different concentrations of cysteine, at 5 and 10 μM. The velocity of the reaction was calculated from the linear part of the time curve (30 s).

2.8. Glutaraldehyde cross-linking

BaSAT was cross-linked using glutaraldehyde. Freshly prepared BaSAT protein was dialyzed against 20 mM HEPES buffer (pH 7.5) overnight before cross-linking. Fifty micrograms of BaSAT was mixed with a final concentration of 60 mM glutaraldehyde, and the reaction was carried out for variable durations of time ranging from 30 s to 60 min. The reaction was stopped using 20 mM Tris–HCl pH 8.0. Samples were mixed with SDS containing loading buffer and analyzed on 10% SDS–PAGE.

2.9. Dynamic light scattering

Freshly prepared BaSAT protein at a concentration of 2.8 mg/ml was used for DLS experiments at room temperature. The buffer used for the protein contains 50 mM Tris–HCl (pH 8.0), 150 mM NaCl, 5% glycerol, and 5 mM β-ME. Buffer solutions were filtered through 0.2-μm filters. The sample was centrifuged at 18000 ×*g* for 60 min and filtered through 0.1-μm filters prior to DLS measurements. The sample was placed in a light-scattering cuvette and exposed to the laser using SpectroSize™ 300 from Nano Biochem Technology, Hamburg. At least 10 measurements of 20 s each were taken.

Co-ordinates and structure factors for native BaSAT and BaSAT-CoA complex were deposited in protein data bank with accession id 4HZC and 4HZD, respectively.

3. Results and discussion

3.1. Structure of BaSAT

The BaSAT protein crystallized in the space group $P2_1$ with 12 monomers arranged in two hexamers in an asymmetric unit. The final model was refined to an R and free R of 18.7% and 24.3%, respectively. The C-terminal end is not fully traced, as there was no electron density for the last 13 residues. Each monomer of BaSAT is composed of two domains: an N-terminal α helix-rich domain and a C-terminal left-handed β-helical (LβH) domain (Fig. 1a). The groove between the two LβH domains from the two adjacent protomers forms the active site. The active site where both serine and cysteine are known to bind is situated between the two adjacent C-terminal domains (Fig. 1b). Three protomers interact with each other, dominated by C-terminal LβH domain interactions, to form a trimeric arrangement. In an each trimer, there are three active sites.

Two trimers associate with each other as a dimer-of-trimeric arrangement to form hexamers. This hexameric state has also been seen in *E. coli* SAT [7] and *H. influenzae* SAT [8] structures. Interestingly, BaSAT is seen as a trimer in gel filtration profiles (Supplementary Fig. 1), while the crystal structure shows it as hexamers. SATs generally exist in oligomeric forms, the hexameric form being a quite common arrangement as have been reported for *E. coli* and *H. influenzae* SATs, while trimeric SAT was reported in *E. histolytica* [9]. The oligomerization of SAT plays an important role in the regulatory mechanism of the cysteine biosynthesis pathway where it is known that complex formation results in decrease in OASS activity [9]. Each monomer in one trimer interacts with the other trimer using hydrophobic interactions at the N-terminal domain, mediated primarily by contacts between helix 2

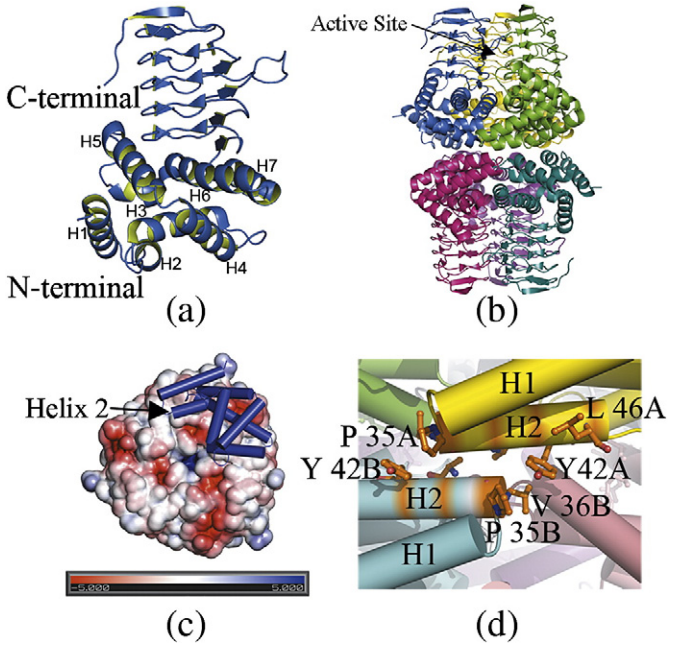

Fig. 1. Overall structure of BaSAT. (a) Side view of monomer of BaSAT showing N-terminal domain consisting mainly of α-helices and the C-terminal catalytic domain consisting of a left-handed β-helix. (b) Side view of the BaSAT hexamer showing the active site between the two adjacent monomers (black arrow). (c) Surface charge distribution image of the N-terminal surface of BaSAT with a monomer of BaSAT superimposed over it to mark the position of helix 2. (d) Helix 2 is involved primarily in hydrophobic interactions, mediated by the labelled amino acids, between the two trimers, hence stabilizing the hexamer.

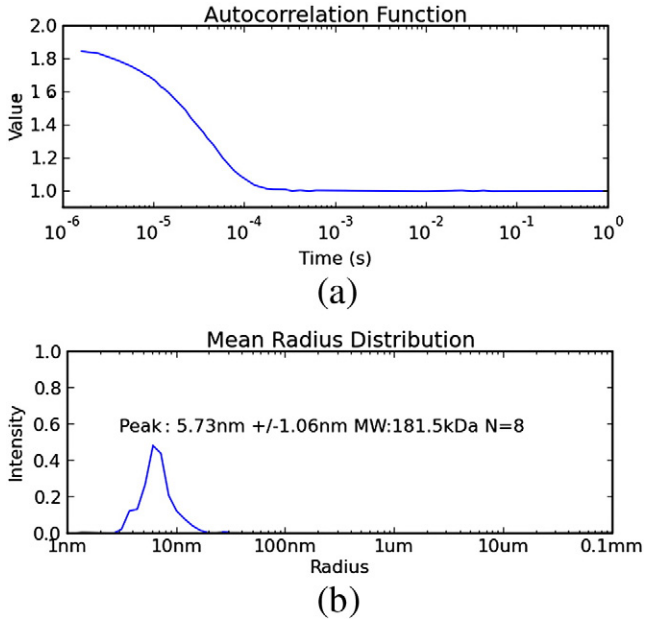

Fig. 2. DLS measurement of BaSAT. The DLS profile shows the hexameric state of the BaSAT. The mono-dispersed peak obtained from hydrodynamic radius of the particle indicates a molecular weight of ~181 kDa; this value, when compared to the monomeric molecular weight of 29.8 kDa, clearly indicates a hexameric state of the protein. A smaller peak is also seen as shoulder at about 4.1 nm, which corresponds to a molecular weight of about 83 kDa and hence represents a smaller fraction of trimeric BaSAT (~90 kDa). (a) Autocorrelation function (*Y*-axis) plotted as a function of time (*X*-axis) and (b) hydrodynamic radii (*X*-axis) plotted as a function of intensity distribution (*Y*-axis).

of one monomer and helix 2 of the other (Fig. 1c). Proline 35A and Val 36A forms hydrophobic interactions with Tyr 42B, as does Val 36B and Pro 35B with Tyr 42A (Fig. 1d).

Gel filtration chromatography, used to purify the BaSAT, indicated a trimeric state (Supplementary Fig. 1a), whereas in the crystal structures it was seen as hexamer. This discrepancy led us to determine the oligomeric state using additional independent techniques. DLS measurements supported the observation that the protein probably exists in equilibrium as both trimer and hexamer. In the solution, the hexameric peak has a radius of 5.73 nm and an average predicted molecular weight of 181 kDa (Fig. 2), but there is also a small peak associated that is seen

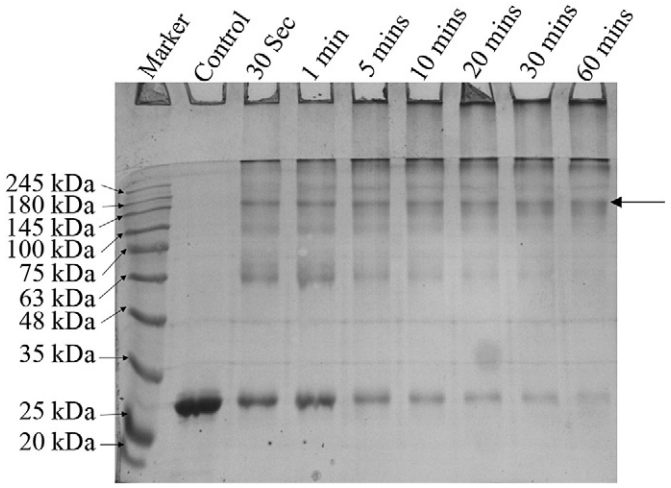

Fig. 3. Glutaraldehyde cross-linking of BaSAT. BaSAT after cross-linking with glutaraldehyde was resolved on 10% SDS–PAGE. Protein bands corresponding to ~180 kDa are visible even after 30-s incubation. Lane two is control showing monomer of BaSAT at ~ 30 kDa.

as a shoulder with a probable radius of 4.1 nm, which approximately corresponds to 83 kDa, close to the molecular weight of BaSAT trimer (~90 kDa). However, the ratio of trimer is very little compared to the hexameric state. Glutaraldehyde is a nonspecific cross-linking agent [33] that has been used by several researchers to analyze the oligomeric state of proteins [34–37]. The cross-linking reactions carried out for 30 s show BaSAT protein bands at the size of dimer, trimer (~90 kDa), and hexamer (~180 kDa). In the subsequent 1- and 5-min incubations of protein and glutaraldehyde, the band corresponding to dimeric and trimeric molecular weight started to disappear and vanished completely at the 10-min incubation. In contrast, the band corresponding to hexameric weight (shown by black arrow) persisted for the entire incubation period (Fig. 3). Most of the protein at the higher time points was seen as a hexamer, and there was also a high molecular weight band. The total surface area calculated using the PDBePISA server [38] of the native BaSAT hexamer is 45600 Å^2, and the total buried surface area is 20400 Å^2, which also suggest that most of the molecule is buried due to the trimer–trimer interactions. The ΔG^{diss} of 109.8 kCal/mol calculated for the BaSAT molecule by the same server suggests stable hexameric assembly. However, taking into consideration the gel filtration results, it seems that the BaSAT stays in trimeric state at low concentrations and in crystal structure, and DLS studies indicate hexameric state as they are performed at higher protein concentrations. These results indicate the BaSAT exists in equilibrium between trimeric and hexameric conformations, most probably depending on the concentration.

3.2. Structure of BaSAT with coenzyme A

BaSAT in complex with coenzyme A (CoA) was crystallized in the R3 space group with two monomers per asymmetric unit. Each of the monomers belongs to a trimer of the hexamer related by crystal symmetry. Coenzyme A is bound in the cleft between C-terminal β helical domains of three equivalent sites of one trimer (Fig. 4a). The omit map calculated confirmed the presence of the ligand (Supplementary Fig. 4). The temperature factors of CoA and omit map indicate that CoA may not be fully occupied. For other equivalent trimer, the electron density at the CoA-binding site was not strong enough for building a CoA molecule. The interactions involved in the binding of CoA are primarily hydrophobic in nature (Fig. 4c). LIGPLOT [39] was used for tracing residues involved in interactions with CoA (Fig. 4d). Several hydrophobic residues at the C-terminus form a cavity, which accommodates CoA. Ala 214A makes a hydrogen bond with the relatively terminal carbonyl oxygen of the CoA pentathenyl arm. The amide group of Ala 232A bonds with the more proximal carbonyl oxygen of the arm, while the carbonyl oxygen of Ala 232A bonds with nitrogen from the CoA adenyl moiety. These hydrogen bonds serve the purpose of stabilizing and orienting the extended chain of CoA at the active site of the SAT (Fig. 4d), which results in the proximity of the acetyl group to active site and subsequently its transfer to substrate serine. The superimposition of the BaSAT-CoA complex with the EhSAT1-serine complex structure (PDB 3Q1X) shows that the extended chain reaches to the active center of the enzyme where the serine is bound. The catalytic core consisting of the His 208, His 223, His 168, and Asp 165 is in bonding position, which facilitates the transfer of the acetyl group to the serine (Fig. 5). His 168 residue can activate the –OH group of the serine, which will act as nucleophile at Acetyl CoA for the generation of a tetrahedral intermediate. The positive charge on the His 168 is stabilized by the carbonyl oxygen of Asp 165. This intermediate is stabilized by the amide group of His 208. Further rearrangement results in the formation of the acetylated serine (O-acetyl serine) with release of CoA (Fig. 5b).

The comparison of BaSAT in the apo and CoA complexed states shows that there is no significant difference between the structures of the protein (RMSD = 0.17 Å for 219 Cα atoms), even at the CoA binding site, indicating lock and key binding without any conformational change. BaSAT-CoA complex has a total surface area of 49600 Å^2 and a

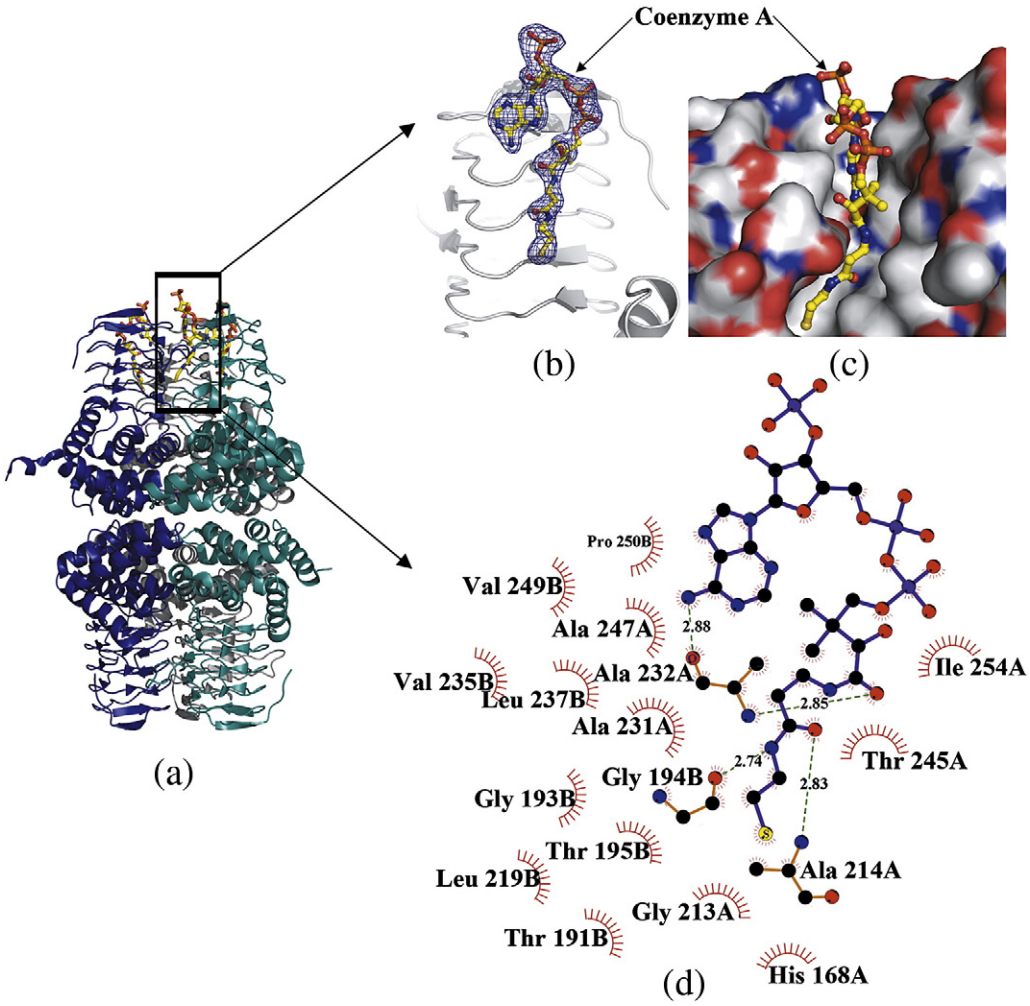

Fig. 4. BaSAT structure in complex with coenzyme A. Coenzyme A is the other product of the reaction of acetyl CoA and serine, where SAT converts serine to *O*-acetylserine. (a) Hexameric BaSAT in complex with coenzyme A. Each CoA molecule is seen binding at three equivalent position between the C-terminals of the adjacent monomers. (b) Coenzyme A is superposed with *2Fo-Fc* electron density (*blue*) at a 0.8 sigma level in the BaSAT-CoA complex structure. (c) Surface representation of the Co-A binding site of BaSAT showing the hydrophobic nature of the cavity required for the binding of coenzyme A. (d) LIGPLOT representation of the interactions of CoA with BaSAT residues. All the interactions are made by hydrophobic residues, of which Ala 232, Gly 194 and Ala 214 are the major contributors.

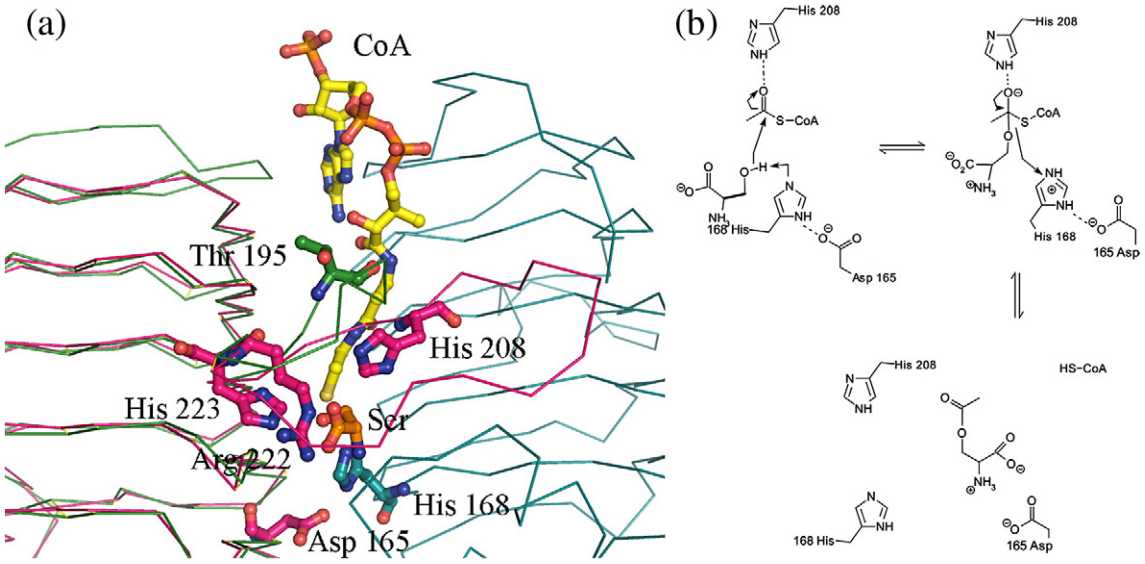

Fig. 5. Visualization of the CoA-serine interaction. (a) Superposition of BaSAT-CoA complex structure with EhSAT1-serine complex structure reveals that the acetyl-CoA is positioned in such a way that the extended arm carrying the acetyl group reaches the active center where the other substrate serine is bound; this serine is flanked by the residues His 208, Arg 222, and His 223, which mediate the transfer of the acetyl group to the serine and result in the formation of the *O*-acetylserine. (b) Schematic representation of proposed mechanism for formation of O-acetyl serine from serine and Acetyl Co-enzyme A in BaSAT.

total buried surface area of 20100 Å^2. Comparing these buried surface area values to the native structure, it is clear that the complex structure also favors the similar hexameric arrangement.

3.3. Comparison with other structures

The amino acid sequence comparison shows that the N-terminal domain of BaSAT has few differences in comparison to *E. coli* SAT, *H. influenzae* SAT, and *G. max* SAT (Fig. 6a). The hydrophobic amino acids are conserved across the N-terminal region in these three SATs, which supports the conclusion that BaSAT, like EcSAT and HiSAT, forms the same hexameric oligomer. The EhSAT structure is very similar to that of BaSAT in the C-terminal domain, but the N-terminal domain is less conserved: helix 4 is straight and continuous in EhSAT but is broken in bacterial SATs, which was responsible for loss of hexamerization in EhSAT [9].

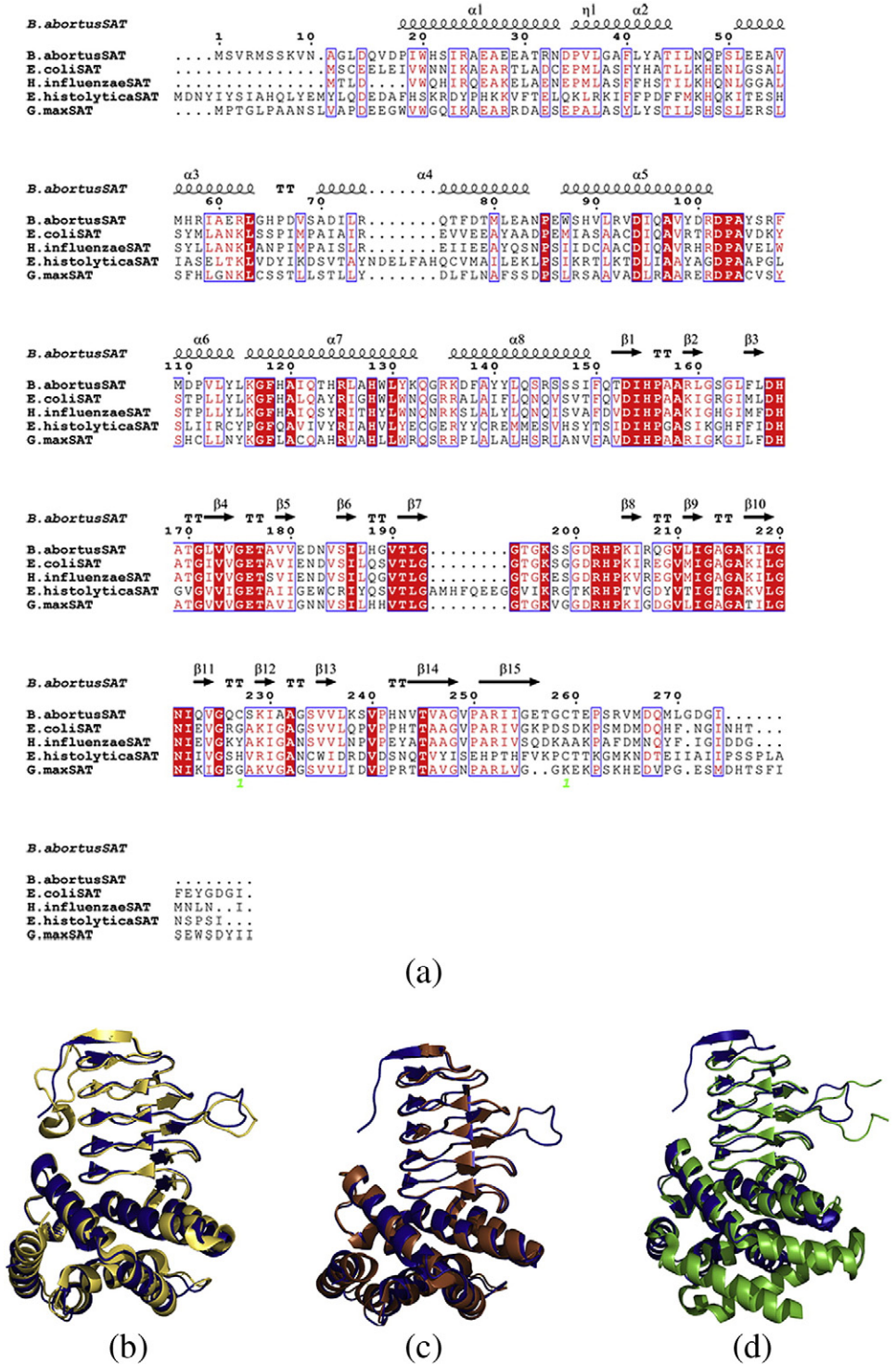

Fig. 6. Sequence alignments of different SAT sequences with BaSAT. (a) Primary amino acid sequence of BaSAT is aligned with amino acid sequence of different SATs for which structure is available. The secondary structures shown above are for BaSAT. Alignment was done using Clustalw, and the figure was prepared using the Escript2.2 program. Structural alignment of BaSAT (blue) with (b) *Brucella melintensis* SAT (magenta), (c) *Escherichia coli* SAT (yellow), (d) *Haemophilus influenzae* SAT (brown), and (e) *Entamoeba histolytica* SAT (green).

The overall architecture of SAT is conserved among the available structures. The N-terminal α-helix-rich domain responsible for oligomerization and the C-terminal β-sheet-rich domain containing the active site are present in all the structures, albeit with some small differences between them. The RMSD of the BaSAT structure is 0.215 Å (for 215 residues) with *B. melintensis* SAT (PDB id 3MC4) (Fig. 6b) and 0.64 Å (for 211 residues) with *E. coli* SAT (PDB id 1T3D) [7] (Fig. 6c). The RMSD is 0.69 Å (for 211 residues) with *H. influenzae* SAT (PDB id 1SST) [8] (Fig. 6d) and 0.71 Å (for 128 residues) with *E. histolytica* SAT (PDB id 3P1B) [9] (Fig. 6e). *G. max* SAT-CoA complex structure (PDB id 4N6B) has RMSD of 0.69 (for 207 residues) with BaSAT-CoA complexed structure. The extended loop is disordered in the *G. max* SAT structure, and Lys 231 side chain is oriented towards the CoA, while equivalent Lys is oriented away in BaSAT structure (Supplementary Fig. 3b). The rest of the equivalent residues are conserved in both the structures.

It was observed that in comparison to bacteria, protozoan parasites have modified the SAT to cater to their oxidative defence requirements [9]. The active site residues are conserved in all SATs with the exception of *E. histolytica* SAT where a His residue is present in the extended loop at 208 position and is known to modify the cysteine binding capacities of the SAT in isoform-dependent manner [40]. It is known that plants such as *Arabidopsis* have at least five subcellular isoforms which behave differentially in response to cysteine feedback inhibition [41].

3.4. Enzyme activity and kinetics study

The activity of BaSAT was determined by measuring the decrease in absorbance at 232 nm due to breakage of the acetyl-CoA thioester bond. The kinetic parameters were calculated from a Michaelis–Menten curve of velocity vs serine concentration using SigmaPlot (Supplementary Fig. 4a). The apparent $K_{m(ser)}$ of the enzyme was calculated to be 127.5 μM (Table 2). The same reaction was repeated in the presence of 5 and 10 μM cysteine, which competitively inhibited the BaSAT according to the increases of the K_m to 192.3 and 278.29 μM, respectively. The apparent $K_{m(CoA)}$ calculated with respect to acetyl CoA is 104.7 μM (Table 2). On addition of cysteine to the reaction, the K_m remains almost the same while the V_{max} increases, showing the mixed type inhibition of acetyl CoA by cysteine (Fig. 1c). Note that, according to previous studies, EcSAT and HiSAT are also competitively inhibited by cysteine. In HiSAT, the binding of cysteine to the active site induces a conformational change in the loop between the β sheets, and this loop also interacts with the C-terminal loop to block the accessibility to the acetyl CoA binding site [9].

4. Conclusion

BaSAT was seen as hexamer in crystal structure; however, the oligomeric state determined by gel filtration profile, chemical cross-linking, and DLS suggests that BaSAT is present in both trimeric and hexameric states in solution. The DLS studies suggest that BaSAt mostly stays as hexamers and crystal structure shows the BaSAT to be hexamer, suggesting that the higher oligomeric state crystallized. The hexameric state is also supported by the buried surface area and free energy calculations. In the crystal structure, hydrophobic interactions between the N-terminal domains of the two trimers are responsible for stabilizing the hexamer. These observations suggest that BaSAT stays in equilibrium between trimer and hexamer; thus, the oligomeric state is mostly dependent on the concentration of the protein. It is important to note that the oligomeric state of the SAT is crucial for the formation of the cysteine synthase complex because if the SAT deviates from the hexameric structure, the cysteine synthase complex formation can be effected [9].

The structure of the complex of BaSAT with coenzyme A and the mode of the binding of CoA is similar to that reported in the *H. influenzae* SAT structure [11]. A recent complex structure of *Glycine max* SAT with CoA also revealed that the overall mechanism of the binding of the CoA to the SAT is conserved across the organisms [10], like *H. influenzae* and *B. abortus*. BaSAT enzyme activity, however, is lower than that for the other reported bacterial SATs.

As seen in the *H. influenzae* SAT-cys complex structure, cysteine inhibits the binding of acetyl CoA by bringing the C-terminal end and the loop near the third coil close to each other to bury the acetyl-CoA binding site [8,9]. Such an interaction, however, was not seen in *E. histolytica*, where cysteine binding has no effect on the acetyl CoA binding site [9,42]. Thus, the regulation of this pathway could be species specific. Moreover, in *A. thaliana*, five subcellular isoforms of SAT have been reported, one of which is in plastids and another in mitochondria [41], and each of these isoforms shows differential feedback regulation. Similarly, each of the three SAT isoforms of *E. histolytica* displays different levels of feedback regulation as well [9,42]. The kinetic studies reveal that the end product cysteine inhibits the binding of substrate serine competitively and shows a mixed type of inhibition for acetyl coenzyme A. Based on the structures, the binding of the acetyl CoA seems to be lock and key binding rather than induced fit. Overall, the structure and function of BaSAT seems to be very similar to EcSAT and HiSAT; however, BaSAT will be the first SAT to show the different oligomeric state, i.e., this molecule seems to be in equilibrium between trimeric–hexameric states.

Supplementary data to this article can be found online at http://dx.doi.org/10.1016/j.bbapap.2014.07.009.

Table 2
Kinetic parameters for BaSAT.

	K_m (μM)	K_m (μM), 5 μM Cys	K_m (μM), 10 μM cys
BaSAT (Ser)	127.5 ± 19.9	192.3 ± 20.2	278.3 ± 31.3
BaSAT (CoA)	104.7 ± 12.5	107.7 ± 28.1	119.4 ± 13.9

The K_m calculate here is apparent K_m.

Acknowledgements

We thank the staff of Beamline 14 at the European synchrotron radiation facility and the Department of Biotechnology, Government of India, for obtaining access to the beamline. We thank Prof. Rakesh Bhatnagar for providing the genomic DNA of *Brucella abortus* strain S19. We thank Dr. Rajesh Pujari and Dr. Divya Goel for help in enzyme activity experiments and critical reading of the manuscript. We thank Prof. Rajeev Bhat, Head of the Department, School of Biotechnology, JNU, for providing access to central instrumentation facility. SK and NK thank University Grants commission (UGC) for fellowship. We thank DST and DBT, Government of India, for funding. We also like to thank institutional grants DST-PURSE, DST-FIST, and UGC Resource Networking.

References

[1] T. Leustek, M.N. Martin, J.A. Bick, J.P. Davies, Pathways and regulation of sulfur metabolism revealed through molecular and genetic studies, Annu. Rev. Plant Physiol. Plant Mol. Biol. 51 (2000) 141–165.
[2] S.K. Hatzios, C.R. Bertozzi, The regulation of sulfur metabolism in *Mycobacterium tuberculosis*, PLoS Pathog. 7 (2011) e1002036.
[3] I.K. Smith, J.F. Thompson, Purification and characterization of L-serine transacetylase and *O*-acetyl-L-serine sulfhydrylase from kidney bean seedlings (*Phaseolus vulgaris*), Biochim. Biophys. Acta 227 (1971) 288–295.
[4] G.E. Ravilious, J.M. Jez, Structural biology of plant sulfur metabolism: from assimilation to biosynthesis, Nat. Prod. Rep. 29 (10) (2012) 1138–1152.
[5] R. Schnell, G. Schneider, Structural enzymology of sulphur metabolism in *Mycobacterium tuberculosis*, Biochem. Biophys. Res. Commun. 396 (2010) 33–38.
[6] M.A. Becker, N.M. Kredich, G.M. Tomkins, The purification and characterization of *O*-acetylserine sulfhydrylase-A from *Salmonella typhimurium*, J. Biol. Chem. 244 (1969) 2418–2427.
[7] V.E. Pye, A.P. Tingey, R.L. Robson, P.C. Moody, The structure and mechanism of serine acetyltransferase from *Escherichia coli*, J. Biol. Chem. 279 (2004) 40729–40736.

[8] J. Gorman, L. Shapiro, Structure of serine acetyltransferase from *Haemophilus influenzae* Rd, Acta Crystallogr. D Biol. Crystallogr. 60 (2004) 1600–1605.
[9] S. Kumar, I. Raj, I. Nagpal, N. Subbarao, S. Gourinath, Structural and biochemical studies of serine acetyltransferase reveal why the parasite *Entamoeba histolytica* cannot form a cysteine synthase complex, J. Biol. Chem. 286 (2011) 12533–12541.
[10] H. Yi, S. Dey, S. Kumaran, S.G. Lee, H.B. Krishnan, J.M. Jez, Structure of soybean serine acetyltransferase and formation of the cysteine regulatory complex as a molecular chaperone, J. Biol. Chem. 288 (2013) 36463–36472.
[11] L.R. Olsen, B. Huang, M.W. Vetting, S.L. Roderick, Structure of serine acetyltransferase in complexes with CoA and its cysteine feedback inhibitor, Biochemistry 43 (2004) 6013–6019.
[12] P.G. Detilleux, B.L. Deyoe, N.F. Cheville, Penetration and intracellular growth of *Brucella abortus* in nonphagocytic cells in vitro, Infect. Immun. 58 (1990) 2320–2328.
[13] G. Pappas, P. Panagopoulou, L. Christou, N. Akritidis, Brucella as a biological weapon, Cell. Mol. Life Sci. 63 (2006) 2229–2236.
[14] C.L. Baldwin, R. Goenka, Host immune responses to the intracellular bacteria Brucella: does the bacteria instruct the host to facilitate chronic infection? Crit. Rev. Immunol. 26 (2006) 407–442.
[15] R.A. Bowden, A. Cloeckaert, M.S. Zygmunt, S. Bernard, G. Dubray, Surface exposure of outer membrane protein and lipopolysaccharide epitopes in *Brucella* species studied by enzyme-linked immunosorbent assay and flow cytometry, Infect. Immun. 63 (1995) 3945–3952.
[16] J. Godfroid, A. Cloeckaert, J.P. Liautard, S. Kohler, D. Fretin, K. Walravens, B. Garin-Bastuji, J.J. Letesson, From the discovery of the Malta fever's agent to the discovery of a marine mammal reservoir, brucellosis has continuously been a re-emerging zoonosis, Vet. Res. 36 (2005) 313–326.
[17] D. Goel, R. Bhatnagar, Intradermal immunization with outer membrane protein 25 protects Balb/c mice from virulent *B. abortus* 544, Mol. Immunol. 51 (2012) 159–168.
[18] N.M. Kredich, M.A. Becker, G.M. Tomkins, Purification and characterization of cysteine synthetase, a bifunctional protein complex, from *Salmonella typhimurium*, J. Biol. Chem. 244 (1969) 2428–2439.
[19] I. Raj, S. Kumar, S. Gourinath, The narrow active-site cleft of *O*-acetylserine sulfhydrylase from Leishmania donovani allows complex formation with serine acetyltransferases with a range of C-terminal sequences, Acta Crystallogr. D 68 (2012).
[20] M.T. Claus, G.E. Zocher, T.H. Maier, G.E. Schulz, Structure of the *O*-acetylserine sulfhydrylase isoenzyme CysM from *Escherichia coli*, Biochemistry 44 (2005) 8620–8626.
[21] R. Schnell, W. Oehlmann, M. Singh, G. Schneider, Structural insights into catalysis and inhibition of *O*-acetylserine sulfhydrylase from *Mycobacterium tuberculosis*, Crystal structures of the enzyme alpha-aminoacrylate intermediate and an enzyme-inhibitor complexJ. Biol. Chem. 282 (2007) 23473–23481.
[22] E.R. Bonner, R.E. Cahoon, S.M. Knapke, J.M. Jez, Molecular basis of cysteine biosynthesis in plants: structural and functional analysis of *O*-acetylserine sulfhydrylase from *Arabidopsis thaliana*, J. Biol. Chem. 280 (2005) 38803–38813.
[23] K. Chinthalapudi, M. Kumar, S. Kumar, S. Jain, N. Alam, S. Gourinath, Crystal structure of native *O*-acetyl-serine sulfhydrylase from *Entamoeba histolytica* and its complex with cysteine: structural evidence for cysteine binding and lack of interactions with serine acetyl transferase, Proteins 72 (2008) 1222–1232.
[24] Z. Otwinowski, W. Minor, Processing of x-ray diffraction data collected in oscillation mode, Methods Enzymol. 276 (1997) 307–326.
[25] B.W. Matthews, Solvent content of protein crystals, J. Mol. Biol. 33 (1968) 491–497.
[26] N. Stein, CHAINSAW: a program for mutating pdb files used as templates in molecular replacement, J. Appl. Crystallogr. 41 (2008) 641–643 (%@ 0021-8898).
[27] A. Vagin, A. Teplyakov, Molecular replacement with MOLREP, Acta Crystallogr. D Biol. Crystallogr. 66 (2010) 22–25.
[28] M.D. Winn, C.C. Ballard, K.D. Cowtan, E.J. Dodson, P. Emsley, P.R. Evans, R.M. Keegan, E.B. Krissinel, A.G. Leslie, A. McCoy, S.J. McNicholas, G.N. Murshudov, N.S. Pannu, E.A. Potterton, H.R. Powell, R.J. Read, A. Vagin, K.S. Wilson, Overview of the CCP4 suite and current developments, Acta Crystallogr. D Biol. Crystallogr. 67 (2011) 235–242.
[29] G.N. Murshudov, P. Skubak, A.A. Lebedev, N.S. Pannu, R.A. Steiner, R.A. Nicholls, M.D. Winn, F. Long, A.A. Vagin, REFMAC5 for the refinement of macromolecular crystal structures, Acta Crystallogr. D Biol. Crystallogr. 67 (2011) 355–367.
[30] P. Emsley, K. Cowtan, Coot: model-building tools for molecular graphics, Acta Crystallogr. D Biol. Crystallogr. 60 (2004) 2126–2132.
[31] P.D. Adams, P.V. Afonine, G. Bunkoczi, V.B. Chen, I.W. Davis, N. Echols, J.J. Headd, L.W. Hung, G.J. Kapral, R.W. Grosse-Kunstleve, A.J. McCoy, N.W. Moriarty, R. Oeffner, R.J. Read, D.C. Richardson, J.S. Richardson, T.C. Terwilliger, P.H. Zwart, PHENIX: a comprehensive Python-based system for macromolecular structure solution, Acta Crystallogr. D Biol. Crystallogr. 66 (2010) 213–221.
[32] G. Langer, S.X. Cohen, V.S. Lamzin, A. Perrakis, Automated macromolecular model building for X-ray crystallography using ARP/wARP version 7, Nat. Protoc. 3 (2008) 1171–1179.
[33] I. Migneault, C. Dartiguenave, M.J. Bertrand, K.C. Waldron, Glutaraldehyde: behavior in aqueous solution, reaction with proteins, and application to enzyme crosslinking, Biotechniques 37 (2004) 790–796 (798–802).
[34] L.H.H. Olde Damink, P.J. Dijkstra, M.J.A. Luyn, P.B. Wachem, P. Nieuwenhuis, J. Feijen, Glutaraldehyde as a crosslinking agent for collagen-based biomaterials, J. Mater. Sci. Mater. Med. 6 (1995) 460–472.
[35] F. Canals, Signal transmission by epidermal growth factor receptor: coincidence of activation and dimerization, Biochemistry 31 (1992) 4493–4501.
[36] E.C. Rabon, S. Bassilian, L.J. Jakobsen, Glutaraldehyde crosslinking analysis of the C12E8 solubilized H,K-ATPase, Biochim. Biophys. Acta 1039 (1990) 277–289.
[37] T. Krupnik, A. Dobrowolski, J.S. Lolkema, Cross-linking of dimeric CitS and GltS transport proteins, Mol. Membr. Biol. 28 (2011) 243–253.
[38] E. Krissinel, K. Henrick, Inference of macromolecular assemblies from crystalline state, J. Mol. Biol. 372 (2007) 774–797.
[39] A.C. Wallace, R.A. Laskowski, J.M. Thornton, LIGPLOT: a program to generate schematic diagrams of protein–ligand interactions, Protein Eng. 8 (1995) 127–134.
[40] S. Kumar, M. Mazumder, S. Dharavath, S. Gourinath, Single residue mutation in active site of serine acetyltransferase isoform 3 from *Entamoeba histolytica* assists in partial regaining of feedback inhibition by cysteine, PLoS One 8 (2013) e55932.
[41] M. Noji, K. Inoue, N. Kimura, A. Gouda, K. Saito, Isoform-dependent differences in feedback regulation and subcellular localization of serine acetyltransferase involved in cysteine biosynthesis from *Arabidopsis thaliana*, J. Biol. Chem. 273 (1998) 32739–32745.
[42] S. Hussain, V. Ali, G. Jeelani, T. Nozaki, Isoform-dependent feedback regulation of serine *O*-acetyltransferase isoenzymes involved in L-cysteine biosynthesis of *Entamoeba histolytica*, Mol. Biochem. Parasitol. 163 (2009) 39–47.